The 2F5 Epitope Is Helical in the HIV-1 Entry Inhibitor T-20[†]

Zohar Biron,[‡] Sanjay Khare,[§] Sabine R. Quadt,[‡] Yehezkiel Hayek,[‡] Fred Naider,[§] and Jacob Anglister*,[‡]

Department of Structural Biology, Weizmann Institute of Science, Rehovot 76100, Israel, and Department of Chemistry and Macromolecular Assemblies Institute, College of Staten Island and the Graduate Center of CUNY, 2800 Victory Boulevard, Staten Island, New York 10314

Received May 18, 2005; Revised Manuscript Received August 17, 2005

ABSTRACT: The HIV-1 envelope glycoprotein gp41 is responsible for viral fusion with the host cell. The fusion process, as well as the full structure of gp41, is not completely understood. One of the strongest inhibitors of HIV-1 fusion is a 36-residue peptide named T-20, $gp41_{(638-673)}$ (Fuzeon, also called Enfuvirtide or DP-178; residues are numbered according to the HXB2 gp160 variant) now used as an anti HIV-1 drug. This peptide also contains the immunogenic sequences that represent the full or partial recognition epitope for the broadly neutralizing human monoclonal antibodies 2F5 and 4E10, respectively. Due to its hydrophobicity, T-20 tends to aggregate at high concentrations in water, and therefore the structure of this molecule in aqueous solution has not been previously determined. We expressed a uniformly $^{13}C/^{15}N$-labeled 42-residue peptide NN-T-20-NITN ($gp41_{636-677}$) and used heteronuclear 2D and 3D NMR methods to determine its structure. Due to the additional gp41-native hydrophilic residues, NN-T-20-NITN dissolved in water, enabling for the first time determination of its secondary structure at near physiological conditions. Our results show that the NN-T-20-NITN peptide is composed of a mostly unstructured N-terminal region and a helical region beginning at the center of T-20 and extending toward the C-terminus. The helical region is found under various conditions and has been observed also in a 13-residue peptide $gp41_{659-671}$. We suggest that this helical conformation is maintained in most of the different tertiary structures of the gp41 envelope protein that form during the process of viral fusion. Accordingly, an important element of the immunogenicity of gp41 and the inhibitory properties of Fuzeon may be the propensity of specific sequences in these polypeptides to assume helical structures.

The penetration of human immunodeficiency virus 1 (HIV-1)[1] into its host cells is mediated by its two envelope glycoproteins, gp41 and gp120. The extracellular protein gp120 is responsible for host recognition by interacting with two receptors of the host cells (CD4 and CCR5 or CXCR4) (*1*). The role of gp41 is to activate the fusion between the membrane of the virus and the membrane of the target cell (*2*). During this process gp41 undergoes a number of conformational changes (*3*, *4*).

gp41 contains several functional domains: the fusion peptide, the fusion peptide proximal domain, the N-helix and C-helix regions that form the core structure of gp41, the loop connecting the N- and C-helices, the C-terminal extracellular membrane proximal domain, the transmembrane domain, and the cytoplasmic tail (Figure 1). The three-dimensional X-ray structure of the HIV-1 gp41 core, composed of the N- and C-helices, revealed a six-helix bundle formed by three C-helices packed on a coiled-coil conformation formed by three N-helices (*5*−*7*). A similar tertiary structure for the gp41 core of the simian immunodeficiency virus (SIV) was determined by multidimensional NMR (*3*). The six-helix bundle structure found in both HIV-1 and SIV gp41 is assumed to be the fusogenic or postfusogenic form of gp41 (*8*).

The C-terminal membrane proximal domain that is flanked by the C-helix and the gp41 transmembrane domain is a relatively conserved region that plays an important role in the fusion process. Deletion of segments within the C-terminal membrane proximal domain or Ala mutations of specific amino acids in this domain (residues W666−I682 of the HXB2 strain of HIV-1) decreased the ability of gp41 to mediate both cell−cell fusion and virus entry and in some cases abolished fusion altogether (*9*, *10*). Furthermore, this region contains the full or partial epitopes of the neutralizing monoclonal antibodies (mAb) 2F5 (*11*), 4E10 (*12*), and Z13 (*13*). These unique antibodies neutralize a broad spectrum of HIV-1 isolates. They, specifically the extensively studied 2F5, are thought to bind the prefusogenic or intermediate forms of gp41, thus preventing viral fusion with the host cell.

[†] This study was supported by NIH Grants GM53329 (J.A.) and GM22086 (F.N.). J.A. is the Dr. Joseph and Ruth Owades Professor of Chemistry and F.N. is the Leonard and Esther Kurtz Term Professor at the College of Staten Island.

* To whom correspondence should be addressed. E-mail: Jacob.Anglister@weizmann.ac.il. Phone: 972-8-9343394. Fax: 972-8-9344136.

[‡] Weizmann Institute of Science.

[§] College of Staten Island and the Graduate Center of CUNY.

[1] Abbreviations: CD, circular dichroism; gp120, the external envelope glycoprotein of HIV-1 with molecular mass of 120 kDa; gp41, the transmembrane envelope glycoprotein of HIV-1 with molecular mass of 41 kDa; $gp41_{636-677}$, a gp41 peptide comprising residues 636−677 from the HXB2 strain; HIV-1, human immunodeficiency virus type 1; NOESY, nuclear Overhauser effect spectroscopy; SIV, simian immunodeficiency virus; mAb, monoclonal antibodies; CNBr, cyanogen bromide; TFA, trifluoroacetic acid.

10.1021/bi0509245 CCC: $30.25
Published on Web 09/24/2005

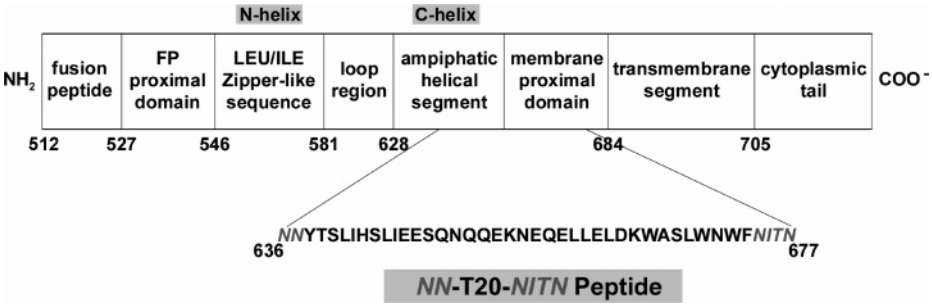

FIGURE 1: Functional regions of the HIV-1 gp41 envelope glycoprotein. Residues are numbered according to the HXB2 gp160 variant. The sequences of T-20 (bold), along with the additional six residues (italic) used in this study, are highlighted.

During the prehairpin intermediate stage, the gp41 ectodomain is available for binding to inhibitor molecules. One of the strongest inhibitors of HIV-1 fusion, now used as an anti-HIV-1 drug, is a 36-residue peptide named T-20 ($gp41_{638-673}$, Fuzeon, also called Enfuvirtide or DP-178) (*14*−*16*). This peptide consists of the C-terminal segment of the C-helix and most of the membrane proximal region of gp41 (Figure 1). T-20 represents a new class of anti-HIV-1 drugs that inhibits the fusion of the virus with its target cells by competitively binding to the N-helix and preventing the formation of the six-helix bundle (*14*, *17*). This proposed mechanism is supported by the finding of T-20-resistant phenotypes of HIV strains that are mutated in their N-helix (*18*). Despite the clinical importance of T-20 and its corresponding region in gp41, the structure of neither has been solved.

The structures of a free 13-residue peptide ($gp41_{659-671}$) containing a segment of T-20 and encompassing most of the 2F5 epitope were solved by NMR at two different conditions (*19*, *20*). The structures of 7- and 17-residue peptides ($gp41_{662-668}$ and $gp41_{654-670}$) in complex with the 2F5 antibody were determined by X-ray crystallography (*21*, *22*). The four structures varied from a 3_{10}-helix (*19*) to a turn (*20*, *21*) to almost an extended conformation (*22*). The crystal structure of the mAb 4E10 epitope ($gp41_{670-678}$, which is downstream of the 2F5 epitope and partially overlaps the C-terminal segment of T-20) in complex with the Fab 4E10 was recently solved and revealed a helical conformation preceded by a short turn formed by N671−W672 (*23*). These results are in good agreement with the helical structure found by NMR in the $gp41_{665-683}$ peptide in dodecylphosphocholine micelle medium (*24*). The structure of the gp41 core composed of N- and C-peptides of different lengths was solved by crystallography. The C-peptide that has the largest overlap with T-20 formed a helix until residue D664 with the last turn in a 3_{10}-helical conformation as frequently observed at the end of helices (*25*).

T-20 forms aggregates above 10 μM concentrations (*9*) and is insoluble in water at the concentrations normally used for NMR structure determination (0.2−2 mM). It was concluded that in 50% aqueous acetonitrile T-20 was predominantly random with a low percentage of α-helix mapped by NMR to E662−N671 (*26*). In this study we partially alleviated the aggregation and solubility problems by elongating T-20 with six additional native residues from gp41. Uniform labeling of the peptide with ^{15}N and $^{13}C/^{15}N$ using an *Escherichia coli* expression system and the use of 3D NMR allowed assignment of most of the NMR spectrum of the peptide in 7% DMSO/93% H_2O and by extension permitted NMR analyses in aqueous buffer. The NMR results suggest that the NN-T-20-NITN peptide is composed of an N-terminal unstructured region and a helical region beginning at the center of T-20 and extending toward the C-terminus. It is likely that the helicity of this domain is an important element of the biological activity of the drug.

EXPERIMENTAL PROCEDURES

Synthesis of NN-T-20-NITN. The 42-residue NN-T-20-NITN peptide (5.12 kDa) corresponding to the sequence NNYTSLIHSLIEESQNQQEKNEQELLELDKWASLWNWFNITN was synthesized using a solid-phase strategy. All reagents and solvents used for the solid-phase peptide synthesis of the 42-amino acid residue fragment were analytical grade and were purchased from Advanced ChemTech (Louisville, KY), Calbiochem-NovaBiochem Corp. (San Diego, CA), VWR Scientific (Piscataway, NJ), and Aldrich (St. Louis, MO). High-performance liquid chromatography grade dichloromethane, acetonitrile, methanol, and water were purchased from VWR Scientific and Fischer Scientific (Springfield, NJ). Automated synthesis of the 42-mer peptide was carried out on an Applied Biosystem 433A peptide synthesizer (Applied Biosystems, Foster City, CA) using a preloaded Fmoc-L-Asn Wang resin (0.56 mmol/g; Advanced Chemtech) on a 0.1 mmol scale. The 0.1 mmol FastMoc chemistry of Applied Biosystems was used for the elongation of the peptide chain with a 2-(1*H*-benzotriazol-1-yl)-1,1,3,3-tetramethyluronium hexafluorophosphate/*N*-hydroxybenzotriazole/diisopropylethylamine-catalyzed coupling step using 10 equiv of protected amino acids.

The chemistry for the synthesis was designed on the basis of the hydrophobic nature of many of its amino acid residues and the length of this peptide. Starting from the carboxyl terminus the first six amino acids were single coupled, amino acids 7−16 were double coupled, amino acids 17−25 were single coupled, and amino acids 26−42 were double coupled to obtain optimum synthesis of the 42-residue peptide. After complete chain assembly, the resin was washed with 1-methyl-2-pyrrolidone and dichloromethane and dried in a vacuum for 4−5 h. The peptide was cleaved from the resin support with simultaneous side chain deprotection using trifluoroacetic acid (10 mL), crystalline phenol (0.75 g), thioanisole (0.5 mL), water (0.5 mL), and 1,2-ethanedithiol (0.25 mL). Filtrates from the cleavage mixture were collected, combined with trifluoroacetic washes of the resin, concentrated under reduced pressure, and treated with cold ether to precipitate the crude product. The yield of crude peptide was 240 mg (47%).

The crude product was checked by analytical HPLC, and three major peaks were observed (data not shown). All three peaks were collected, lyophilized, and sent for ESI-MS. The peak eluting at 40.6% acetonitrile in water (using a shallow gradient of 37−52% in 10 min and a C18 analytical column) was found to have the correct MS value (MW, 5121.61 Da; MS, 5120.80 Da; Mass Facility, Hunter College/CUNY, New York). To obtain milligram quantities of peptide, 20 mg of crude peptide was injected into a VYDAC C4 reversed-phase column (VYDAC 214TP102205), and purification was accomplished using a shallow gradient of 34−41% acetonitrile with 0.1% of TFA over 60 min. The final peptide was greater than 98% homogeneous on analytical HPLC and had the correct mass as judged by MALDI mass spectrometry.

Construction of the NN-T-20-NITN Peptide Expression Vector. TrpΔLE polypeptide (*27*) DNA with a His tag at the N-terminus was inserted between the *Nde*I and *Bam*HI sites of pET24a (Novagen) and used as a construct for a carrier protein. The coding DNA for the Met-NN-T-20-NITN peptide including two TAA stop codons was attached to the TrpΔLE polypeptide sequence using *Hin*dIII and *Bam*HI restriction sites. This construct codes for a fusion protein containing a total of 165 amino acid residues, 123 from the carrier protein TrpΔLE polypeptide (including the His tag and Met residues) and the 42 residues of the NN-T-20-NITN peptide.

Expression of the NN-T-20-NITN Fusion Protein. *E. coli* BL21-Gold(DE3)pLysS competent cells (Stratagene) were transformed with a plasmid containing the sequence coding for the NN-T-20-NITN fusion protein. Bacteria containing this plasmid were grown in ^{15}N-labeled and ^{15}N/^{13}C-labeled rich media (using isotope-enriched Celtone medium) supplemented with 50 μg/mL kanamycin, RPMI 1640 vitamin cocktail (Gibco), 1 mM $MgSO_4$, and 50 mM K_2HPO_4 to a cell density of OD_{595} 0.7−1.0. Expression was induced by adding 1 mM IPTG followed by incubation for 3 h at 37 °C and shaking at 225 rpm. The bacteria were collected by centrifugation (8000 rpm for 30 min), frozen, and stored overnight at −80 °C. The overexpressed fusion protein was isolated from the cells in the form of inclusion bodies. The cells were suspended in 20 mL of 50 mM Tris-HCl, pH 8.0, 0.5 mM EDTA, and 0.5 M NaCl (washing buffer) and sonicated for 3 min. The cell lysate was spun at 13000 rpm for 10 min at 4 °C, and the pellet containing the inclusion bodies was washed twice with 20 mL of washing buffer. The inclusion bodies were gradually dissolved in 9 M urea containing 50 mM glycine and 0.5 M NaCl. The undissolved debris was removed from the supernatant by centrifugation at 13000 rpm (Sorvall SS-34) for 30 min. The supernatant was then dialyzed against 50 mM NH_4HCO_3 and lyophilized, yielding more then 90% pure fusion protein (∼80 mg/L).

NN-T-20-NITN Peptide Cleavage and Purification. The peptide was released from the fusion protein using cyanogen bromide (CNBr) cleavage (*28*). A stock solution of 5 M CNBr in acetonitrile was used. The cleavage was carried out for 8 h in 70% trifluoroacetic acid (TFA) at room temperature. Upon completion of the reaction 10 volumes of water was added to the sample, and it was then lyophilized to complete dryness. This procedure was further optimized, by using methyl *tert*-butyl ether in order to stop the cleavage reaction and to precipitate the peptide. After overnight cooling at −20 °C the ether solution was centrifuged at 12000 rpm for 30 min. The product was dissolved in dimethylformamide (DMF) and acetonitrile with 0.1% TFA and purified by HPLC on a VYDAC C4 reversed-phase column,(VYDAC 214TP102205) to greater than 95% homogeneity. Amino acid analysis and mass spectrometry confirmed the composition and molecular weight of the labeled peptide (for the ^{15}N sample the molecular mass was 5177 Da corresponding to 93% labeling; for the ^{15}N/^{13}C sample the molecular mass was 5400 Da corresponding to 97% labeling). The yields of purified NN-T-20-NITN were ∼7 mg/L.

Circular Dichroism. CD spectra of the peptide were recorded at various temperatures on an AVIV model 62 DS CD instrument (AVIV associates, Lakewood, NJ). The ellipticity was measured at 0.5 nm intervals, and three measurements were averaged for each temperature. To follow the melting of the peptide conformation, the ellipticity was measured at 220 nm over the temperature range 275−363 K with 0.5 K intervals. The peptide concentration was determined from UV measurements at 280 nm using an extinction coefficient of 5800 M^{-1} cm^{-1} per tryptophan residue and 1280 M^{-1} cm^{-1} per tyrosine residue. The synthetic peptide was dissolved in water at 10 μM concentration, and the pH was adjusted to 7.7 using 1.0 M ammonium hydroxide (addition of Tris-HCl as a buffer increased the noise level considerably). CD intensities are expressed as mean residue ellipticities (deg cm^2 $dmol^{-1}$).

Sedimentation Equilibrium Measurement. Sedimentation equilibrium measurements were conducted in a Beckman XL-A analytical ultracentrifuge. Sample concentration was limited to 60 μM due to the high extinction coefficient of the peptide. The buffer and the pH conditions were similar to those in the NMR measurements (50 mM unlabeled Tris-HCl buffer, pH 7.7) excluding DMSO. Equilibrium data were collected at 35000 rpm at 277 K. The concentration gradient was monitored by the absorbance at 280 nm. Equilibrium was reached after an overnight run.

NMR Measurements on the NN-T-20-NITN Peptide. NMR spectra of the NN-T-20-NITN peptide were measured using 0.4 mM samples with 50 mM deuterated Tris-HCl buffer in 93% H_2O solution containing 7% deuterated DMSO, pH 7.7, or using a 0.1 mM sample in 50 mM deuterated Tris-HCl buffer, pH 7.7, without DMSO. The spectra were recorded on a Bruker DMX-500 MHz equipped with a cryoprobe and on a Bruker DRX-800 MHz spectrometer. Data were processed and analyzed using XWINNMR (Bruker), NMRPipe (*29*), and NMRVIEW (*30*) programs. Homonuclear 2D TOCSY and NOESY experiments were measured on unlabeled peptide using 60 and 200 ms mixing periods, respectively. Water flip-back was used to improve the signal-to-noise ratio for the amide cross-peaks (*31*). For the two-dimensional (2D) [^{1}H,^{15}N] HSQC and ^{1}H−^{15}N NOE (*32*) experiments 200 t_1 increments at a sweep width of 17 ppm and 2048 t_2 points at a sweep width of 12 ppm were used. The following three-dimensional experiments were carried out for sequential assignment: three-dimensional HNCO, CBCA(CO)NH, and HN(CA)CO experiments (*33*) were run on the DMX 500 MHz spectrometer. The HNCA (*34*, *35*) and the ^{15}N-separated TOCSY experiment that was acquired with a 60 ms mixing time were run on the DRX-800 MHz spectrometer. Connectivities and internuclear distances were obtained from a 3D ^{15}N-separated [^{1}H,^{1}H] NOESY (*36*) with

a mixing time of 200 ms. Typical carrier positions for all experiments were 119.5 ppm for ^{15}N, 174 ppm for ^{13}CO, 54 ppm for $^{13}C\alpha$, 45 ppm for $^{13}C\alpha/^{13}C\beta$, and 4.973 ppm for ^{1}H. For the determination of the HN temperature coefficient seven 3D HNCO experiments were acquired at seven different temperatures around 277 K, with a minimum temperature of 273 K and a maximum temperature of 285 K.

For the determination of chemical shift indices the difference in ppm between the measured chemical shifts and the random coil chemical shifts was calculated and decisions as to secondary structure based on threshold values given in the literature (*37*). The percent helix for each residue was calculated using the equation:

$$(\delta_{meas} - \delta_{random})/(\delta_{helix} - \delta_{random})$$

where δ_{meas} = measured chemical shift for a specific type of amino acid, δ_{random} = the random coil chemical shift for that type of amino acid, and δ_{helix} = the average chemical shift for that type of amino acid in a helical conformation. The approach follows that developed according to ref *37*.

RESULTS

Sample Optimization. Previous attempts to obtain NMR spectra of T-20 ($gp41_{638-673}$) in aqueous solution were unsuccessful due to aggregation (*26*). Although shorter peptides containing portions of the T-20 sequence had been studied, we reasoned that more meaningful results would be obtained by extending the peptide at the termini using native residues. To increase the solubility of T-20, we decided to study a slightly elongated gp41 peptide ($gp41_{636-677}$), which included two asparagine residues ($N_{636}N_{637}$) at the N-terminus and four residues ($N_{674}ITN_{677}$) at the C-terminus. The solubility of the NN-T-20-NITN peptide improved at slightly basic pH (7.7). At pH 7 and below the solubility decreased considerably. The increased solubility above neutral pH is not surprising considering that NN-T-20-NITN has a net charge of −5.

Despite the considerable improvement in solubility, relatively broad spectral lines were seen in the NMR spectra of 0.4 mM peptide samples, suggesting some aggregation. Further improvement of the spectra was achieved by the addition of low concentrations of DMSO (7% v:v, 2% mol/mol). It has been demonstrated that DMSO, unlike other organic solvents, does not contribute to the formation of helical conformations (*38*). Furthermore, DMSO in high concentrations was shown to interfere with hydrogen bond formation and by that destroy secondary structures (*38*, *39*). It has been suggested that DMSO/water mixtures may be generally useful for NMR investigations of aggregating peptides, providing information on the structural preferences in aqueous environment without the complication of diminished H-bond acceptor properties (associated with organic solvents such as acetonitrile) and helicity induction associated with aqueous solutions of fluoro alcohols/water solutions (*40*). Indeed, the addition of acetonitrile increased considerably the helicity of T-20 (*26*) and NN-T-20-NITN (data not shown). In contrast, an analogue peptide, $gp41_{647-677}$, did not show any change in proton chemical shift in H_2O and 7% DMSO/93% H_2O (data not shown), thus validating our approach. On the basis of these observations we conducted

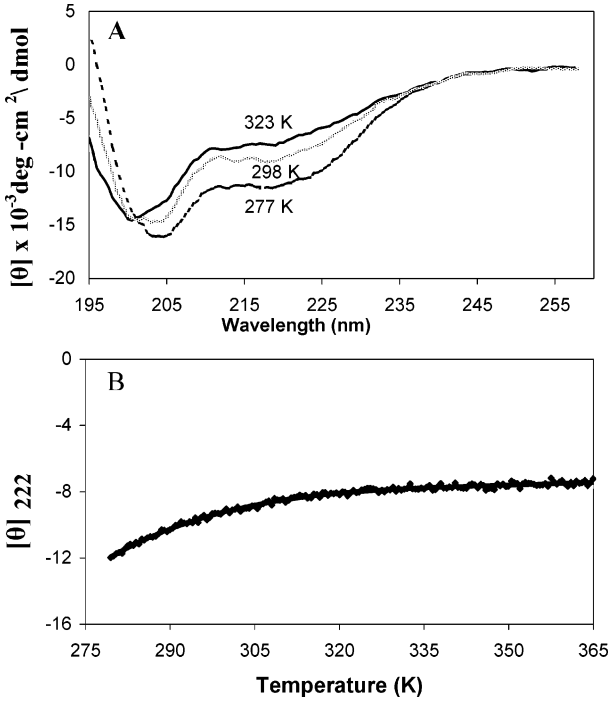

FIGURE 2: Circular dichroism of the NN-T-20-NITN peptide in H_2O at pH 7.7. (A) CD spectra of NN-T-20-NITN measured at 277, 298, and 323 K. (B) Thermal unfolding transition of the NN-T-20-NITN peptide measured at 220 nm. The peptide was dissolved in water at a concentration of 10 μM, and the pH was adjusted to 7.7 by the addition of 1 M ammonium hydroxide solution.

a detailed NMR analysis of NN-T20-NITN in 7%DMSO/water. Comparative studies in 100% aqueous buffer (vide infra) at a lower concentration of NN-T-20-NITN demonstrate that our conclusions are valid for the peptide in water.

Equilibrium Sedimentation of the NN-T-20-NITN Peptide in Aqueous Solution. The molecular mass of the peptide was determined using sedimentation equilibrium at 277 K to assess the oligomerization state of the peptide. Due to the high extinction coefficient at 280 nm, the molecular mass was determined using a 60 μM solution of NN-T-20-NITN in water. The estimated MW of the peptide was found to be 5450 Da, in good agreement with the expected mass of monomer (5.12 kDa). Unlike in the NMR experiments DMSO was not used to prevent aggregation in the sedimentation experiment because it absorbs strongly and prevents detection of the peptide.

Circular Dichroism of the NN-T-20-NITN ($gp41_{636-677}$) Peptide. The circular dichroism (CD) spectrum of $gp41_{636-677}$ was measured in water (without DMSO) to evaluate the secondary structure of the peptide. The peptide concentration was 10 μM. The CD curve at 277 K was characterized by a negative shoulder between approximately 215 and 225 nm and a minimum centered at 205 nm. At wavelengths below 200 nm the ellipticities trended toward positive values. A ratio of $[\theta]_{222}/[\theta]_{205} = 0.7$ was measured (Figure 2A). Very similar CD spectra, having a minimum centered at 205 nm, were also reported for T-20 by others (*9*, *26*, *41*, *42*). The shape and intensity of the CD patterns were similar, but not identical, to those recently reported for short peptides assuming mostly the 3_{10}-helical conformation (*19*, *43*, *44*). The CD spectrum of a 3_{10}-helix is characterized by a minimum between 202 and 206 nm and a ratio $R = [\Theta]_{222}/[\Theta]_{205}$ between 0.15 and 0.4 (*43*, *44*) while values closer to

1 are typical for an α-helix. The stronger shoulder centered at 222 nm observed for NN-T-20-NITN indicates a partial α-helical conformation. The shift of the minima from 205.5 nm at 277 K to 202.5 nm at 323 K and the gradual decrease of the ellipticity at 220 nm from -12×10^{-3} deg·cm^2·dmol^{-1} at 277 K to an asymptotic value of -8×10^{-3} deg·cm^2·dmol^{-1} (reached above 325 K) (Figure 2) suggest that the helicity of the peptide decreases but does not disappear as the temperature increases.

Chemical Shift Assignment of NN-T-20-NITN. To evaluate the structure of NN-T-20-NITN in highly aqueous conditions, we used NMR measurements at 277 K as the CD results suggested that higher percentages of regular secondary structures were present at this low temperature. The HN−HN interactions in NOESY experiments were also observed best at 277 K, suggesting a relatively stable structure at this temperature. At higher temperatures the amide proton NOEs were considerably weaker probably due to a combination of faster exchange with solvent protons and increased mobility. To obtain sharper lines at the concentrations required for NMR measurements, 7% DMSO was added to the peptide samples. In the preliminary stages of the study, we used a chemically synthesized unlabeled 42-residue NN-T-20-NITN peptide. Usually, the structure of peptides of this size (5.12 kDa) can be solved without labeling with ^{13}C and ^{15}N isotopes. However, results from 2D homonuclear NOESY and 2D homonuclear TOCSY spectra showed severe overlap of resonances in the amide region. Moreover, the measured T_2 relaxation time of the amide protons at the optimal temperature (277 K) was 18 ms. The short T_2 resulted in considerable line broadening and consequently limited the resolution. We, therefore, were forced to use ^{15}N- and ^{13}C/^{15}N-labeled peptides for sequential assignment and NOE measurements.

Poor dispersion of nitrogens and protons was observed in the 2D ^{15}N,^{1}H HSQC spectrum of NN-T-20-NITN, typical for helical and unstructured conformations. About 70% of the sequential assignments were obtained using HNCA and CBCA(CO)NH spectra. The ^{15}N-separated TOCSY and the ^{15}N-separated NOESY spectra extended and verified the assignments. Nearly complete backbone assignment was obtained using HNCO and HN(CA)CO experiments. Only the resonances of amide protons of the first three residues (7%) were not assigned due to fast exchange with water. We were also able to assign 90% (38 of 42) of the carbonyl backbone atoms, 93% (39/42) of the $^{13}C_\alpha$ atoms, and 88% (37/42) of the $^{13}C_\beta$ atoms (a table summarizing the chemical shift assignment is presented in the Supporting Information).

Secondary Structure of NN-T-20-NITN by NMR. (A) Chemical Shift Indices. For unstructured "random coil" polypeptides it has long been recognized that the chemical shift of the H_α, C_α, C_β, and CO carbons of a given residue is largely independent of the nature of neighboring residues in the peptide, and random coil shifts have been reported for all amino acids (*45*). In contrast, in proteins and structured peptides the $^{1}H_\alpha$, $^{13}C_\alpha$, $^{13}C_\beta$, and ^{13}CO chemical shifts are influenced mainly by backbone geometry and, therefore, are the most reliable indicators of the secondary structure (*46*, *47*). Positive deviations for $^{13}C_\alpha$ and ^{13}CO and negative deviation for $^{1}H_\alpha$ and $^{13}C_\beta$ chemical shifts are typical of a helical conformation (*46*, *48*). In 7% DMSO/93% water at 277 K the deviation from random coil values for the $^{13}C_\alpha$ carbon chemical shift from residue E657 to residue L669 clearly indicates the formation of a rather stable helical conformation in this region of T-20 (Figure 3A). Analysis of the H_α and CO chemical shifts measured under identical conditions also reveals a helix beginning at E657 and extending toward the carboxyl terminus (Figure 3B,C). The ratio between the deviation from random coil values of the $^{13}C_\alpha$ chemical shift and the average deviation from a random coil value for the given amino acid in a helical conformation can be used to estimate the population of helical conformers in peptides in a residue-specific manner (*37*). Using this approach we estimated that at 277 K in 7% DMSO/93% H_2O 60% of the peptide molecules populate a helical conformation in the E657−L669 segment and 20% and 30% of the molecules populate a helical conformation at the segments S640−N656 and W670−F673, respectively (Figure 3D). The segment N674−N677 is unstructured.

To determine whether DMSO influenced the conformation of NN-T-20-NITN, assignments were obtained using CBCA(CO)NH and HNCO spectra measured at 0.1 mM peptide concentration in 50 mM deuterated Tris-HCl buffer, pH 7.7, without DMSO at 277 K. Most of the cross-peaks could be observed despite the lower concentration of the peptide, and the similarity between the spectra recorded with and without DMSO enabled sequential assignment for most of the backbone nuclei. Figure 3D,E compares the helix percentage obtained at 277 K in the presence and absence of DMSO. The data indicate that the population of the peptide that assumes a helical conformation for segment E657−L669 is slightly increased in the absence of DMSO. Backbone assignments were also obtained at 303 K using CBCA(CO)NH and HNCO spectra measured for 0.1 mM NN-T-20-NITN in 50 mM deuterated Tris-HCl buffer, pH 7.7, without DMSO. Both the C_α (Figure 3F) and CO (data not shown) chemical shift indices reveal that in the buffered water the peptide segment E657−L669 is somewhat less structured at 303 K in comparison to 277 K. Nevertheless, in the buffered water at 303 K we estimate that the E657−L669 segment of NN-T-20-NITN is 40% helical on average. This result is in agreement with the CD results that indicated significant helicity (about 33% helix for the entire peptide) at 310 K (Figure 2).

(B) TALOS Data Base Analysis. To achieve further structural information from the chemical shift assignment, we utilized the TALOS program (*49*). The deviations of the chemical shifts from random coil values, on which the TALOS program is based, are used for secondary structure determination of both peptides and proteins (*37*, *50*). The retrieved ϕ and ψ angles for residues E657−L669 correspond well to typical helical values (Figure 4). Residues Y638−N656, however, did not show values typical for any protein from the database, suggesting again that this segment does not exhibit a well-defined secondary structure.

(C) NOESY Connectivities. Analysis of the 3D ^{15}N-separated [^{1}H−^{1}H] NOESY spectrum revealed 15 $d_{NN}(i,i+1)$ sequential connectivities and 7 medium range connectivities, 5 $d_{\alpha N}(i,i+3)$ connectivities between residues L669−W672, W666−L669, L663−W666, N656−E659, and K655−Q658, and 2 $d_{\alpha N}(i,i+2)$ between residues W666−S668 and N656−Q658, all in the segment of the peptide between Q653−N677 (Figure 3). Despite the use of heteronuclear NMR severe overlap was observed in the ^{15}N-separated NOESY

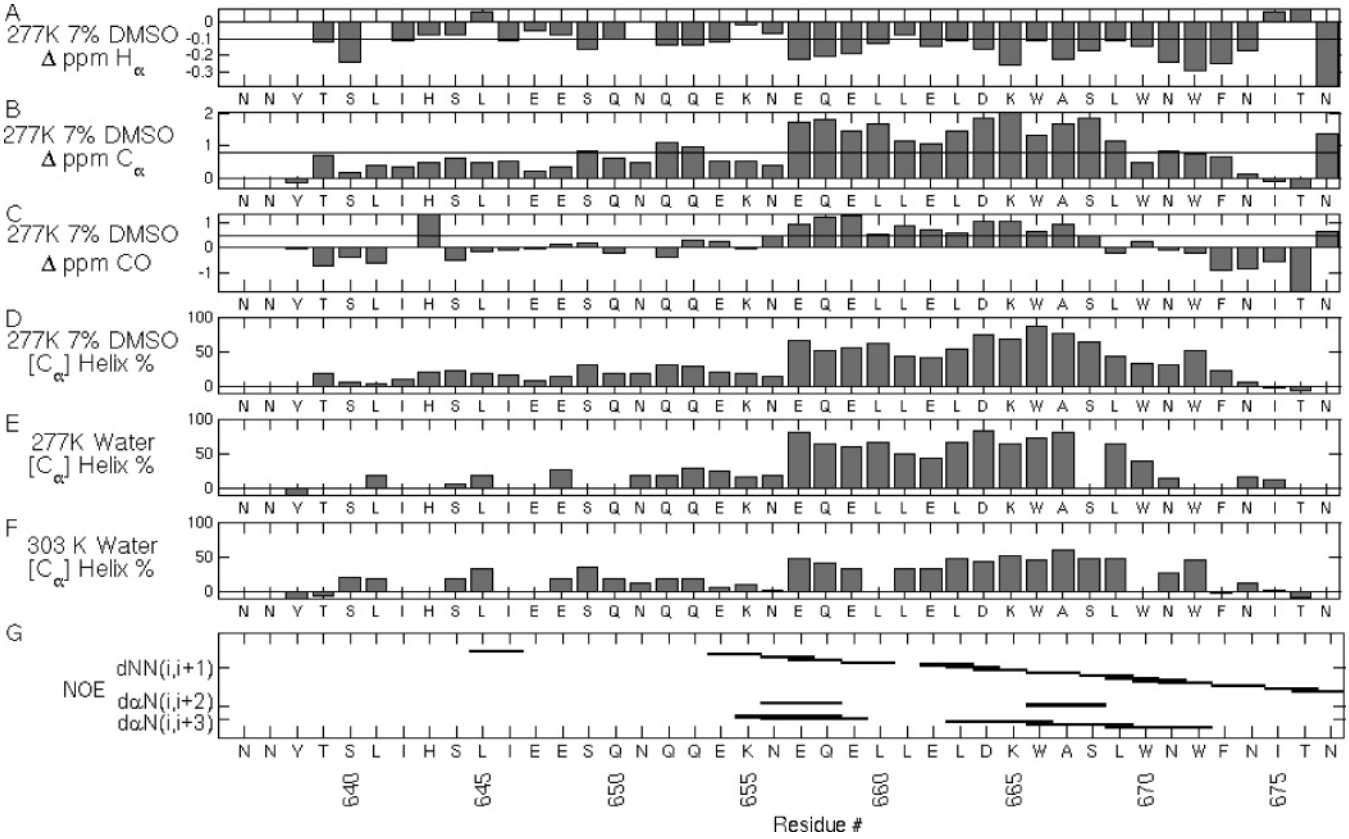

FIGURE 3: Chemical shift indices, percentage of helical conformation, and NOE interactions for the NN-T-20-NITN peptide in aqueous media at pH 7.7. All of the data were collected using 50 mM *d*-Tris-HCl, pH 7.7, as the buffer. (A−C) $^{1}H_{\alpha}$, $^{13}C_{\alpha}$, and ^{13}CO chemical shift deviations from random coil chemical shifts in the NN-T-20-NITN peptide in 7% DMSO/93% H_2O at 277 K. The cutoff values for deviations indicating helical conformations are represented by solid lines. (D), (E), and (F) plot the helix percentage of each residue under various conditions determined using the method of Wishart et al. (*37*) (see Experimental Procedures): (D) 277 K in 7% DMSO/93% H_2O; (E) NN-T-20-NITN peptide in 5% D_2O/95% H_2O, 277 K, in water; (F) NN-T-20-NITN peptide in 5% D_2O/95% H_2O, 303 K. (G) NOE interactions were extracted from 3D ^{15}N-separated NOESY spectra for the peptide in 7% DMSO/93% H_2O.

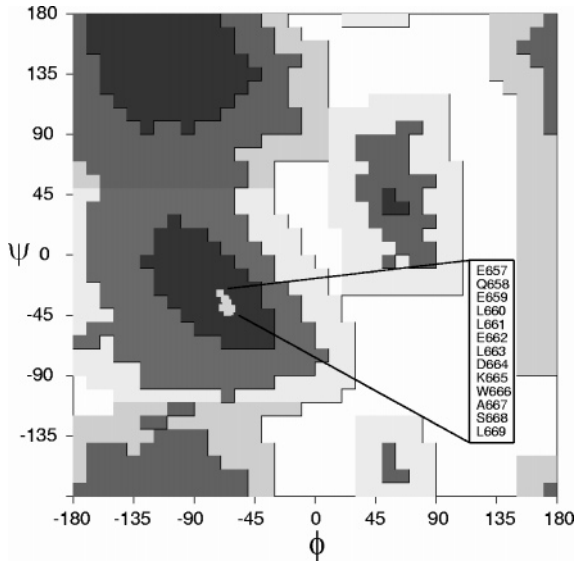

FIGURE 4: Ramachandran plot of the ϕ and ψ angles of NN-T-20-NITN deduced from the chemical shifts of the peptide measured in 7% DMSO/93% H_2O, pH 7.7, at 277 K using TALOS. The gray square represents the ϕ and ψ angles for residues E657−L669, which exhibit values inside the allowed helical region. The estimated error in the deduced dihedral angle is not more than ±16°.

spectrum (Figure 5), preventing the unambiguous assignment of a large number of medium-range NOEs (Figure 5). The observation of several $d_{\alpha N}(i,i+3)$ interactions suggests a significant population in a helical conformation for the Q655−N672 region of NN-T-20-NITN. The unambiguous assignment of only two $d_{\alpha N}(i,i+2)$ does not enable us to differentiate between a 3_{10}-helix and an α-helical conformation. Residues Y638−Q654 in the peptide do not exhibit any medium-range interactions in the NOESY spectrum, again indicating that the N-terminus of the peptide is mostly unstructured. Despite the small number of unambiguosly assigned medium-range NOEs, we attempted to calculate a structure using the CNS program (Crystallography and NMR System) (*51*). To calculate the structure of the Q650−N677 segment of the NN-T-20-NITN peptide, 185 distance constraints (35 of them are medium range) and 30 dihedral angles derived from TALOS were used (Supporting Information). The 25 structures with the lowest energy (from 100 structures without violations) were chosen for statistical analyses. A helical segment is observed (Supporting Information) for the segment E657−L669 with a backbone RMSD of 2 Å.

(D) Temperature Coefficient Analysis. An additional indicator for secondary structure is the existence of hydrogen bonds. The temperature-dependent changes in the amide proton chemical shift (as long as the protein is folded throughout the temperature range of the measurements) are linear, and the temperature coefficients range between −16 to +2 ppb/K (*52*). Cierpicki and Otlewski showed that

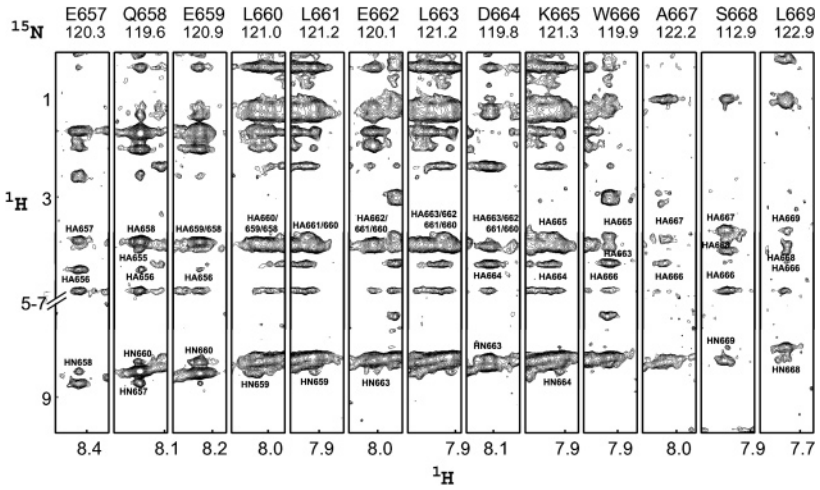

FIGURE 5: ^{N}H strips for residues E657−L669 obtained from the 3D ^{15}N-separated NOESY spectrum of NN-T-20-NITN. The ^{15}N-separated NOESY spectrum was acquired using a 0.4 mM uniformly ^{15}N-labeled sample with 50 mM *d*-Tris-HCl buffer and 7% DMSO/93% H_2O at pH 7.7, 277 K, on a Bruker DRX-800 MHz spectrometer. The mixing period was 200 ms. The region between 5 and 7 ppm was cut from the spectrum for simplification.

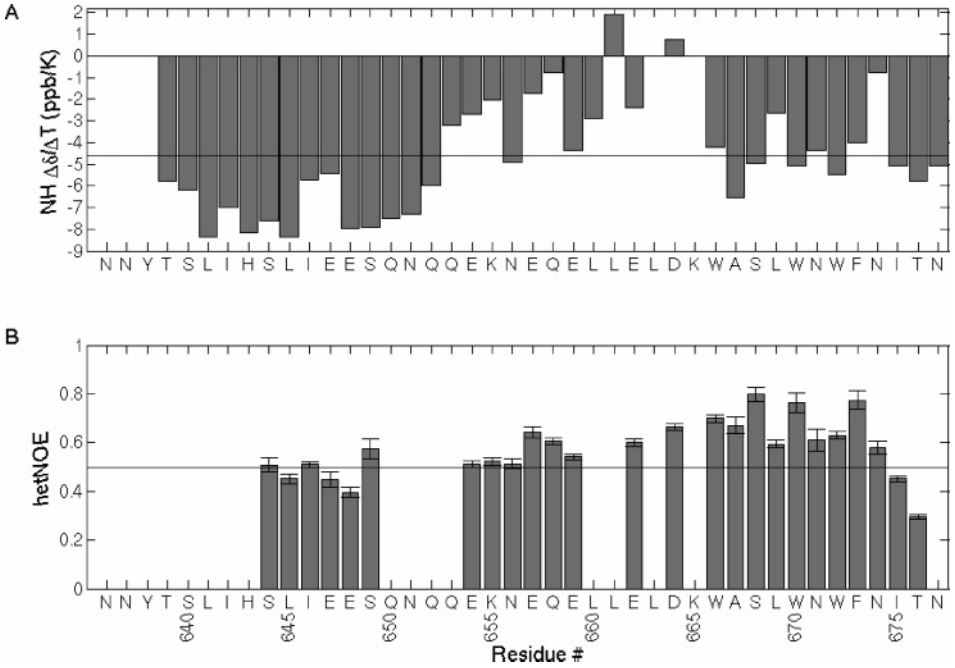

FIGURE 6: Amide proton temperature coefficients and ^{1}H−^{15}N NOE values for NN-T-20-NITN in 50 mM *d*-Tris-HCl and 7% DMSO/93% H_2O at pH 7.7. (A) Temperature coefficients of the amide protons of each residue. The line at −4.6 ppb/K corresponds to the upper threshold value used as an indicator for hydrogen bonding (*53*). (B) ^{1}H−^{15}N heteronuclear NOEs measured at 277 K.

hydrogen-bonded NHs in proteins usually exhibit a high percentage of HN temperature coefficients more positive than −4.6 ppb/K (*53*). We assigned the backbone amide proton chemical shifts for NN-T-20-NITN in 7% DMSO/93% water at six different temperatures between 273 and 285 K. Plots of these chemical shifts at different temperatures were linear, allowing extraction of temperature coefficients (data not shown). Residues Q653−W666 exhibited the most positive δHN/δT values, and 11/12 residues (92%) have temperature coefficients significantly more positive than −4.6 ppb/K, thus supporting the formation of hydrogen bonds by residues in this region of the NN-T-20-NITN peptide (Figure 6). Interestingly, on the basis of the NH temperature coefficients the region between A667−N674 contains a mixture of protected and nonprotected protons, with 4 of the 8 residues (50%) in that region having δNH/δT values more positive than the −4.6 ppb/K threshold. All residues in the N-terminal part of the peptide upstream of Q652 show coefficients significantly more negative than the −4.6 threshold (Figure 6).

(E) Heteronuclear ^{1}H−^{15}N NOE. ^{1}H−^{15}N NOEs of NN-T-20-NITN in 7% DMSO/93% water at 273 K were measured to assess local motions in the peptide. Some of the residues could not be measured due to overlap in the HN region. The relaxation data indicate that the largest heteronuclear NOEs are observed for NHs in the E657−F673 region (Figure 6B) and that these NOEs approach the limiting value of 0.8 observed for well-structured segments

of proteins (*54*). This is consistent with a greater rigidification of this region of NN-DP-178-NITN in comparison to the rest of the peptide.

DISCUSSION

Previous attempts to study the structure of the T-20 peptide in water were stymied by its poor solubility, tendency to aggregate, and the severe overlap found in the NH region of the spectrum. Accordingly, it was previously studied by NMR in 50% acetonitrile, a condition which was shown by CD to stabilize a helical conformation in T-20 (data not shown and Figure 3 in ref *26*). On the basis of a CD analysis it was concluded that, in aqueous buffer at 298 K and close to neutral pH, T-20 is unstructured (*26*). No NMR data supported this conclusion, and CD spectra of T-20 at 10−50 μM in PBS buffer (pH 7.0−7.4) at various temperatures from 274 to 293 K exhibited significant ellipticity at 222 nm suggestive of some helicity. To provide insights into structural tendencies of specific residues of T-20, we circumvented the solubility problems at the concentration required for NMR measurements by elongating T-20 with native polar residues and incorporating ^{13}C and ^{15}N isotopes. This strategy enabled us for the first time to study in detail its structure in aqueous solution.

The present CD and NMR measurements support the conclusion that a continuous segment comprising the center and a major component of the C-terminal half of NN-T-20-NITN, a therapeutically relevant peptide, has significant helical tendencies in aqueous solution. The CD spectrum of NN-T-20-NITN suggests that the peptide may contain a mixture of 3_{10}- and α-helical conformations as well as unstructured segments. NMR was used to map these helices to specific residues. The heteronuclear chemical shifts (C_α and CO) provide strong evidence for a helix beginning at E657 and continuing until at least L669 (Figure 3B,C). Use of these chemical shifts allowed us to estimate the percentage of helical residues within the conformational distribution of NN-T-20-NITN. The E657−L669 segment was calculated to be 60% helical at 277 K in 7% DMSO/93% water (Figure 3D). Strikingly, this segment of T-20 remained 40% helical in 100% aqueous buffer at 303 K (Figure 3F). The same approach indicated that residues S640−N656 and W670−F673 are more than 70% disordered in 7% DMSO/93% water at 277 K. The NOE connectivities are consistent with a helical region beginning at the center of T-20 and extending toward the C-terminus but are not sufficient to map the segments that adopt a 3_{10}-helix and those that adopt an α-helical conformation nor to calculate a high-resolution structure. Temperature coefficients and heteronuclear NOEs also support hydrogen bonding and structure beginning at the center and extending toward the carboxyl terminus of the peptide (Figure 6). Despite the fact that amide proton coefficients more positive than −4.6 ppb/K were used as the cutoff for prediction of hydrogen bonds, a number of hydrogen-bonded protons in α-helical segments of the proteins surveyed exhibited coefficients between −7 and −5 ppb/K (*53*). Thus, we believe that the rather negative coefficient found for A667 is not indicative of a break in the helix and that we can rely on the chemical shift indices to define the limits of the helix. On the basis of our analysis, for the first time a detailed picture of the structural elements present for T-20 in water has emerged. The tendency of T-20 in water to form a helical structure beginning at its center and extending toward the C-terminal end may be relevant to both drug design and the development of effective vaccines.

One might question whether the additional residues have a significant influence on the structure of the T-20 core. The CD spectrum of the elongated peptide (NN-T-20-NITN) in water at 298 K, pH 7.8 (Figure 2), is similar to other reported CD spectra of T-20 (*19*, *26*, *43*, *44*). The small variations between these spectra might reflect small differences in the sample conditions such as pH, salt concentration, or temperature. Asn and Thr have low helix propensities, and it is, as observed by our NMR study, unlikely that they assume a helical structure (*55*). Nevertheless, the carboxyl-terminal extension could stabilize the helix formed by the residues near the center of T-20.

Our results for the structure of NN-T-20-NITN in 7% DMSO/93% water and in aqueous buffer are not in good agreement with a recent crystal structure which concluded that $gp41_{654-670}$ in complex with 2F5 was in an extended structure (*22*). It is somewhat curious that the core structure determined for the postfusion hexahelical bundle composed of $gp41_{628-664}$ and the structure of a central segment extending to the C-terminal strand of NN-T-20-NITN are both helical while that of $gp41_{654-670}$ bound to antibody 2F5 is extended. Perhaps the different conformations observed in NN-T-20-NITN and in the crystal structure of the 2F5 complex represent the conformational diversity of this gp41 segment in the resting virus, during the binding and fusion processes and in the postfusion state.

With respect to the extended structure found for the 2F5-bound $gp41_{657-670}$, we previously suggested that most of this segment is an autonomous folding unit (*19*) that forms an intrinsically stable 3_{10}-helix due to a combination of hydrophobic and electrostatic factors that result in stabilizing local interactions. The present study provides additional evidence that, in the context of the NN-T-20-NITN peptide, residues corresponding to $gp41_{657-669}$ have significant helical tendencies in water. Autonomous folding units probably serve as nucleation sites during protein folding (*56*−*58*), and it is very likely that the region in gp41 corresponding to E657−L669 adopts helical structures similar to those found in the $gp41_{659-671}$ peptide and in NN-T-20-NITN (*59*−*61*). Thus, it is not obvious why or when gp41 would provide the conformational surface leading to the generation of a 2F5 binding site that would recognize an extended peptide topology. It appears that it would be prudent to consider the inherent helicity of the membrane proximal domain of gp41 in the development of strategies for vaccine design.

Until very recently the accepted model for T-20 inhibition suggested attachment of T-20 to the prefusogenic state of gp41 (*41*), thus preventing attainment of the hexahelical bundle required for viral fusion. The importance of T-20 helicity in this process was supported by studies on variously *i*,*i*+7 cross-linked ($gp41_{638-664}$) peptides with enhanced α-helicity (*62*). Further support for the importance of the helicity of T-20 was obtained from a recent examination of the differential inhibition of HIV-1 and SIV envelope-mediated cell fusion by C34 peptides (residues 628−661 of the transmembrane envelope glycoprotein, partially overlapping T-20) derived from diverse strains of HIV-1, HIV-2,

and SIV suggesting that the inhibitory properties of these peptides were correlated with their helical propensities (*63*).

In conclusion, the findings of the present study provide spectroscopic evidence that an extended region at the C-terminal part and near the center of NN-T-20-NITN exists in a helix or incipient helix under nearly physiological conditions. Taken together with findings of others, it is likely that the ability to form this helix is correlated to the biological properties of T-20. Such information may be useful in guiding future attempts at improving the therapeutic indices of this molecule.

ACKNOWLEDGMENT

We are most grateful to Professor Peter S. Kim for giving us the TrpΔLE vector for expressing the peptide and to Dr. Naama Kessler for most helpful advice on the expression and purification of the NN-T-20-NITN peptide.

SUPPORTING INFORMATION AVAILABLE

Two tables listing chemical shift assignments and NMR constraints and structural statistics for the NN-T-20-NITN peptide and one figure showing an ensemble of 25 lowest energy structures of the Q650−N677 segment of the NN-T-20-NITN peptide. This material is available free of charge via the Internet at http://pubs.acs.org.

REFERENCES

1. Dragic, T., Litwin, V., Allaway, G. P., Martin, S. R., Huang, Y., Nagashima, K. A., Cayanan, C., Maddon, P. J., Koup, R. A., Moore, J. P., and Paxton, W. A. (1996) HIV-entry into CD4+ cells is mediated by the chemokine receptor CC-CKR-5, *Nature 381*, 667−673.
2. Eckert, D. M., and Kim, P. S. (2001) Mechanisms of viral membrane fusion and its inhibition, *Annu. Rev. Biochem. 70*, 777−810.
3. Caffrey, M., Cai, M., Kaufman, J., Stahl, S. J., Wingfield, P. T., Covell, D. G., Gronenborn, A. M., and Clore, G. M. (1998) Three-dimensional solution structure of the 44 kDa ectodomain of SIV gp41, *EMBO J. 17*, 4572−4584.
4. Colman, P. M., and Lawrence, M. C. (2003) The structural biology of type I viral membrane fusion, *Nat. Rev. Mol. Cell. Biol. 4*, 309−319.
5. Chan, D. C., Fass, D., Berger, J. M., and Kim, P. S. (1997) Core structure of gp41 from the HIV envelope glycoprotein, *Cell 89*, 263−273.
6. Weissenhorn, W., Dessen, A., Harrison, S. C., Skehel, J. J., and Wiley, D. C. (1997) Atomic structure of the ectodomain from HIV-1 gp41, *Nature 387*, 426−430.
7. Tan, K., Liu, J., Wang, J., Shen, S., and Lu, M. (1997) Atomic structure of a thermostable subdomain of HIV-1 gp41, *Proc. Natl. Acad. Sci. U.S.A. 94*, 12303−12308.
8. Chan, D. C., and Kim, P. S. (1998) HIV entry and its inhibition, *Cell 93*, 681−684.
9. Lawless, M. K., Barney, S., Guthrie, K. I., Bucy, T. B., Petteway, S. R., Jr., and Merutka, G. (1996) HIV-1 membrane fusion mechanism: structural studies of the interactions between biologically-active peptides from gp41, *Biochemistry 35*, 13697−13708.
10. Salzwedel, K., West, J. T., and Hunter, E. (1999) A conserved tryptophan-rich motif in the membrane-proximal region of the human immunodeficiency virus type 1 gp41 ectodomain is important for Env-mediated fusion and virus infectivity, *J. Virol. 73*, 2469−2480.
11. Muster, T., Steindl, F., Purtscher, M., Trkola, A., Klima, A., Himmler, G., Ruker, F., and Katinger, H. (1993) A conserved neutralizing epitope on gp41 of human immunodeficiency virus type 1, *J. Virol. 67*, 6642−6647.
12. Stiegler, G., Kunert, R., Purtscher, M., Wolbank, S., Voglauer, R., Steindl, F., and Katinger, H. (2001) A potent cross-clade neutralizing human monoclonal antibody against a novel epitope on gp41 of human immunodeficiency virus type 1, *AIDS Res. Hum. Retroviruses 17*, 1757−1765.
13. Zwick, M. B., Labrijn, A. F., Wang, M., Spenlehauer, C., Saphire, E. O., Binley, J. M., Moore, J. P., Stiegler, G., Katinger, H., Burton, D. R., and Parren, P. W. (2001) Broadly neutralizing antibodies targeted to the membrane-proximal external region of human immunodeficiency virus type 1 glycoprotein gp41, *J. Virol. 75*, 10892−10905.
14. Wild, C. T., Shugars, D. C., Greenwell, T. K., McDanal, C. B., and Matthews, T. J. (1994) Peptides corresponding to a predictive alpha-helical domain of human immunodeficiency virus type 1 gp41 are potent inhibitors of virus infection, *Proc. Natl. Acad. Sci. U.S.A. 91*, 9770−9774.
15. De Clercq, E. (2002) Highlights in the development of new antiviral agents, *Mini Rev. Med. Chem. 2*, 163−175.
16. Kilby, J. M., Lalezari, J. P., Eron, J. J., Carlson, M., Cohen, C., Arduino, R. C., Goodgame, J. C., Gallant, J. E., Volberding, P., Murphy, R. L., Valentine, F., Saag, M. S., Nelson, E. L., Sista, P. R., and Dusek, A. (2002) The safety, plasma pharmacokinetics, and antiviral activity of subcutaneous enfuvirtide (T-20), a peptide inhibitor of gp41-mediated virus fusion, in HIV-infected adults, *AIDS Res. Hum. Retroviruses 18*, 685−693.
17. Kilgore, N. R., Salzwedel, K., Reddick, M., Allaway, G. P., and Wild, C. T. (2003) Direct evidence that C-peptide inhibitors of human immunodeficiency virus type 1 entry bind to the gp41 N-helical domain in receptor-activated viral envelope, *J. Virol. 77*, 7669−7672.
18. Rimsky, L. T., Shugars, D. C., and Matthews, T. J. (1998) Determinants of human immunodeficiency virus type 1 resistance to gp41-derived inhibitory peptides, *J. Virol. 72*, 986−993.
19. Biron, Z., Khare, S., Samson, A. O., Hayek, Y., Naider, F., and Anglister, J. (2002) A monomeric 3(10)-helix is formed in water by a 13-residue peptide representing the neutralizing determinant of HIV-1 on gp41, *Biochemistry 41*, 12687−12696.
20. Barbato, G., Bianchi, E., Ingallinella, P., Hurni, W. H., Miller, M. D., Ciliberto, G., Cortese, R., Bazzo, R., Shiver, J. W., and Pessi, A. (2003) Structural analysis of the epitope of the anti-HIV antibody 2F5 sheds light into its mechanism of neutralization and HIV fusion, *J. Mol. Biol. 330*, 1101−1115.
21. Pai, E. F., Klein, M. H., Chong, P., and Pedyczak, A. (2000) *in World Intellectual Property Organization*.
22. Ofek, G., Tang, M., Sambor, A., Katinger, H., Mascola, J. R., Wyatt, R., and Kwong, P. D. (2004) Structure and mechanistic analysis of the anti-human immunodeficiency virus type 1 antibody 2F5 in complex with its gp41 epitope, *J. Virol. 78*, 10724−10737.
23. Cardoso, R. M., Zwick, M. B., Stanfield, R. L., Kunert, R., Binley, J. M., Katinger, H., Burton, D. R., and Wilson, I. A. (2005) Broadly neutralizing anti-HIV antibody 4E10 recognizes a helical conformation of a highly conserved fusion-associated motif in gp41, *Immunity 22*, 163−173.
24. Schibli, D. J., Montelaro, R. C., and Vogel, H. J. (2001) The membrane-proximal tryptophan-rich region of the HIV glycoprotein, gp41, forms a well-defined helix in dodecylphosphocholine micelles, *Biochemistry 40*, 9570−9578.
25. Armen, R., Alonso, D. O., and Daggett, V. (2003) The role of alpha-, 3(10)-, and pi-helix in helix to coil transitions, *Protein Sci. 12*, 1145−1157.
26. Joyce, J. G., Hurni, W. M., Bogusky, M. J., Garsky, V. M., Liang, X., Citron, M. P., Danzeisen, R. C., Miller, M. D., Shiver, J. W., and Keller, P. M. (2002) Enhancement of alpha-helicity in the HIV-1 inhibitory peptide DP178 leads to an increased affinity for human monoclonal antibody 2F5 but does not elicit neutralizing responses in vitro. Implications for vaccine design, *J. Biol. Chem. 277*, 45811−45820.
27. Blacklow, S. C., and Kim, P. S. (1996) Protein folding and calcium binding defects arising from familial hypercholesterolemia mutations of the LDL receptor, *Nat. Struct. Biol. 3*, 758−762.
28. Gross, E. (1967) The cyanogen bromide reaction, *Methods Enzymol. 11*, 238−255.
29. Delaglio, F., Grzesiek, S., Vuister, G. W., Zhu, G., Pfeifer, J., and Bax, A. (1995) NMRPipe: a multidimensional spectral processing system based on UNIX pipes, *J. Biomol. NMR 6*, 277−293.
30. Johnson, B. A., and Blevins, R. A. (1994) NMR view—a computer-program for the visualization and analysis of NMR data, *J. Biomol. NMR 4*, 603−614.
31. Grzesiek, S., and Bax, A. (1993) The importance of not saturating H_2O in protein NMR—application to sensitivity enhancement and NOE measurements, *J. Am. Chem. Soc. 115*, 12593−12594.

32. Grzesiek, S., and Bax, A. (1993) Measurement of amide proton exchange rates and NOEs with water in $^{13}C/^{15}N$-enriched calcineurin B, *J. Biomol. NMR 3*, 627−638.
33. Clubb, R. T., Thanabal, V., and Wagner, G. (1992) A constant-time three-dimensional triple resonance pulse scheme to correlate intra-residue ^{1}HN, ^{15}N and ^{13}C chemical shifts in ^{15}N-^{13}C labeled proteins, *J. Magn. Reson. 97*, 213−217.
34. Grzesiek, S., and Bax, A. (1992) Inproved 3D triple resonance techniques applied to a 31 kDa protein, *J. Magn. Reson. 96*, 432−440.
35. Ikura, M., Kay, L. E., and Bax, A. (1990) A novel approach for sequential assignment of ^{1}H, ^{13}C, and ^{15}N spectra, *Biochemistry 29*, 4659−4667.
36. Marion, D., Driscoll, P. C., Kay, L. E., Wingfield, P. T., Bax, A., Gronenborn, A. M., and Clore, G. M. (1989) Overcoming the overlap problem in the assignment of ^{1}H NMR spectra of larger proteins by use of three-dimensional heteronuclear ^{1}H-^{15}N Hartmann−Hahn-multiple quantum coherence and nuclear Overhauser-multiple quantum coherence spectroscopy: application to interleukin 1 beta, *Biochemistry 28*, 6150−6156.
37. Wishart, D. S., and Sykes, B. D. (1994) Chemical shifts as a tool for structure determination, *Methods Enzymol. 239*, 363−392.
38. Jackson, M., and Mantsch, H. H. (1991) Beware of proteins in DMSO, *Biochim. Biophys. Acta 1078*, 231−235.
39. Goodman, M., Verdini, A. S., Toniolo, C., Phillips, W. D., and Bovey, F. A. (1969) Sensitive criteria for the critical size for helix formation in oligopeptides, *Proc. Natl. Acad. Sci. U.S.A. 64*, 444−450.
40. Hudson, F. M., and Andersen, N. H. (2004) Exenatide: NMR/CD evaluation of the medium dependence of conformation and aggregation state, *Biopolymers 76*, 298−308.
41. Kliger, Y., and Shai, Y. (2000) Inhibition of HIV-1 entry before gp41 folds into its fusion-active conformation, *J. Mol. Biol. 295*, 163−168.
42. Mobley, P. W., Pilpa, R., Brown, C., Waring, A. J., and Gordon, L. M. (2001) Membrane-perturbing domains of HIV type 1 glycoprotein 41, *AIDS Res. Hum. Retroviruses 17*, 311−327.
43. Toniolo, C., Polese, A., Formaggio, F., Crisma, M., and Kamphuis, J. (1996) Circular dichroism spectrum of peptide 3_{10}-helix, *J. Am. Chem. Soc 118*, 2744−2745.
44. Formaggio, F., Crisma, M., Rossi, P., Scrimin, P., Kaptein, B., Broxterman, Q. B., Kamphuis, J., and Toniolo, C. (2000) The first water-soluble 3(10)-helical peptides, *Chemistry 6*, 4498−4504.
45. Wüthrich, K. (1986) *NMR of proteins and nucleic acids*, John Wiley, New York.
46. Spera, S., and Bax, A. (1991) Emprical correlation between protein backbone conformation and Ca and Cb nuclear magnetic resonance chemical shifts, *J. Am. Chem. Soc. 113*, 5490−5492.
47. Wishart, D. S., and Sykes, B. D. (1994) The ^{13}C chemical-shift index: a simple method for the identification of protein secondary structure using ^{13}C chemical-shift data, *J. Biomol. NMR 4*, 171−180.
48. Kuszewski, J., Qin, J., Gronenborn, A. M., and Clore, G. M. (1995) The impact of direct refinement against ^{13}C alpha and ^{13}C beta chemical shifts on protein structure determination by NMR, *J. Magn. Reson. B 106*, 92−96.
49. Cornilescu, G., Delaglio, F., and Bax, A. (1999) Protein backbone angle restraints from searching a database for chemical shift and sequence homology, *J. Biomol. NMR 13*, 289−302.
50. Case, D. A., Dyson, H. J., and Wright, P. E. (1994) Use of chemical shifts and coupling constants in nuclear magnetic resonance structural studies on peptides and proteins, *Methods Enzymol. 239*, 392−416.
51. Brunger, A. T., Adams, P. D., Clore, G. M., DeLano, W. L., Gros, P., Grosse-Kunstleve, R. W., Jiang, J. S., Kuszewski, J., Nilges, M., Pannu, N. S., Read, R. J., Rice, L. M., Simonson, T., and Warren, G. L. (1998) Crystallography & NMR system: A new software suite for macromolecular structure determination, *Acta Crystallogr., Sect. D: Biol. Crystallogr. 54* (Part 5), 905−921.
52. Baxter, N. J., and Williamson, M. P. (1997) Temperature dependence of ^{1}H chemical shifts in proteins, *J. Biomol. NMR 9*, 359−369.
53. Cierpicki, T., and Otlewski, J. (2001) Amide proton temperature coefficients as hydrogen bond indicators in proteins, *J. Biomol. NMR 21*, 249−261.
54. Kay, L. E., Torchia, D. A., and Bax, A. (1989) Backbone dynamics of proteins as studied by ^{15}N inverse detected heteronuclear NMR spectroscopy: application to staphylococcal nuclease, *Biochemistry 28*, 8972−8979.
55. Chou, P. Y., and Fasman, G. D. (1974) Conformational parameters for amino acids in helical, beta-sheet, and random coil regions calculated from proteins, *Biochemistry 13*, 211−222.
56. Chakrabartty, A., and Baldwin, R. L. (1995) Stability of alpha-helices, *Adv. Protein Chem. 46*, 141−176.
57. Shoemaker, K. R., Fairman, R., Kim, P. S., York, E. J., Stewart, J. M., and Baldwin, R. L. (1987) The C-peptide helix from ribonuclease A considered as an autonomous folding unit, *Cold Spring Harbor Symp. Quant. Biol. 52*, 391−398.
58. Baldwin, R. L., and Rose, G. D. (1999) Is protein folding hierarchic? I. Local structure and peptide folding, *Trends Biochem. Sci. 24*, 26−33.
59. Dyson, H. J., Lerner, R. A., and Wright, P. E. (1988) The physical basis for induction of protein-reactive antipeptide antibodies, *Annu. Rev. Biophys. Biophys. Chem. 17*, 305−324.
60. Munoz, V., and Serrano, L. (1996) Local versus nonlocal interactions in protein folding and stability—an experimentalist's point of view, *Folding Des. 1*, R71−R77.
61. Serrano, L. (2000) The relationship between sequence and structure in elementary folding units, *Adv. Protein Chem. 53*, 49−85.
62. Judice, J. K., Tom, J. Y., Huang, W., Wrin, T., Vennari, J., Petropoulos, C. J., and McDowell, R. S. (1997) Inhibition of HIV type 1 infectivity by constrained alpha-helical peptides: implications for the viral fusion mechanism, *Proc. Natl. Acad. Sci. U.S.A. 94*, 13426−13430.
63. Gustchina, E., Hummer, G., Bewley, C. A., and Clore, G. M. (2005) Differential inhibition of HIV-1 and SIV envelope-mediated cell fusion by C34 peptides derived from the C-terminal heptad repeat of gp41 from diverse strains of HIV-1, HIV-2, and SIV, *J. Med. Chem. 48*, 3036−3044.

BI0509245